Silicon (2023) 15:1701–1724
https://doi.org/10.1007/s12633-022-02097-5

ORIGINAL PAPER

# Influence of Argon Gas Flow Rate on Oxygen and Carbon Impurities Concentration in Multicrystalline Silicon Grown by Directional Solidification Furnace: Numerical and Experimental Investigation

**S. Sugunraj[1,2] · G. Aravindan[1,2] · M. Srinivasan[1,2] · P. Ramasamy[1,2]**

Received: 16 May 2022 / Accepted: 1 September 2022 / Published online: 27 September 2022


**Abstract**
The quality of the multi-crystalline silicon ingot mainly depends on the defects and impurity distribution. The impurities originate from the various furnace parts and feedstock. The argon gas which acts as carrier gas plays an important role to reduce the chemical reaction inside the furnace. The reduction of carbon and oxygen concentration results in the reduction of SiO, CO and SiC formation. Various argon gas flow rates (5 LPM to 30 LPM) are simulated and C, O, CO and SiO concentrations were analysed. By increasing the argon gas flow rate, the SiO gas in the melt-free surface gets reduced from 6.9E2 to 5.1E1ppma. Also, it prevents CO gas formation in the melt-free surface. Oxygen concentration is lower than the concentration required for LID for 25 LPM and 30 LPM. From the 20 LPM, mc-Si ingot has Carbon concentration lower than the critical concentration required for SiC formation. The experimental result of 25 LPM Argon gas flow rate is compared with simulation results.

**Keywords** Argon gas · Directional solidification · Multi-crystalline silicon · Carbon and oxygen impurity · Chemical reaction

## 1 Introduction

Nowadays, solar cell is one of the important sources for the electricity production. Around the world, many researchers are working in different types of solar cells in order to produce high conversion efficiency. There are three generations of solar cells available in the photovoltaic (PV) market. Silicon based solar cells are dominant in the PV market due to its efficiency with low manufacturing cost. Silicon based solar cells can be divided into two major parts known as monocrystalline silicon (mono-Si, $25.6 \pm 0.5\%$) solar cell and multi-crystalline silicon (mc-Si, $21.25 \pm 0.4\%$) solar cell [1]. Directional solidification (DS) growth technique is used to grow mc-Si ingot. One of the main challenges in the mc-Si ingot growth is to control the impurity concentration, because it affects the efficiency of the solar cell. The melt-crystal interface and melt flow have been studied from 0 to 30 litter per minute (LPM) argon gas flow rate (AGFR). Thermal buoyancy force is enhanced and the direction of the melt flow is driven by the argon gas flow. Above 30 LPM, the central part of the melt is quickly solidified due to cooling effect of argon gas [2]. The effect of AGFR was investigated during the cooling process at 60 to 200 min by varying the velocity from 0.05 to 0.6 m/s [3]. Quality of the mono-crystalline silicon ingot was improved by the gas controlled hot zone furnace [4]. Gas guidance system was used in the DS process to reduce the formation of CO by 31% [5]. Argon gas flow and furnace pressure of the DS furnace were studied [6]. From the argon gas injector, the argon gas flow was improved. From this modification mc-Si ingot impurity concentration was reduced [7]. The AGFR affects the temperature distribution during the casting process and it affects the quality of the ingot [8]. The crucible rotation reduces the oxygen evaporation [9]. Carbon and oxygen concentration of mc-Si ingot was reduced by using the molybdenum gas shield [10]. The investigation of melt flow pattern

✉ M. Srinivasan
srinisastri@gmail.com

[1] Department of Physics, Sri Sivasubramaniya Nadar College of Engineering, Chennai 603110, India

[2] Research Centre, Sri Sivasubramaniya Nadar College of Engineering, Chennai 603110, India

and oxygen concentration were studied in CZ process. From that investigation, by increasing the AGFR the melt flow pattern and oxygen concentration was affected [11]. Tungsten cover is used to reduce the CO formation in the DS process. It helps to reduce the carbon concentration [12]. DS Furnace pressure was studied. From that investigation it was concluded that during the CO gas transport, the convection process dominates at minimum furnace pressure and the diffusion process dominates at maximum furnace pressure [13]. If the oxygen concentration level above 1.5E17 atoms/cm$^3$ (3.3ppma) in the crystal, it will encourage the light induced degradation (LID) [14]. If carbon concentration is above 1E16 atoms/cm$^3$, it will enhance the precipitation of oxygen and also reduce the minority carrier life time [13]. During the crystal growth process, if the carbon concentration is above 1.3E17atoms/cm3, it will enhance the SiC precipitation [15].

Many researchers have modified the furnace parts to reduce the impurity concentration. Our main aim is to grow the mc-Si ingot below the critical level of both LID and SiC formation. In the DS furnace, the SiO gas is carried outside the furnace with the help of argon gas. In this work, we have numerically investigated the AGFR to optimize the quality of the ingot in generation 1 (G1) DS furnace and the suitable AGFR is implemented in the experiment. In both cases, there is no crucible rotation applied in the growth process. Experimentally, the impurity concentrations are investigated with the help of FTIR measurement. The impact of AGFR on ingot growth conditions is investigated. Simulation work was done with the help of CGSim software. Their results are compared.

## 2 Model Description

Figure 1 shows the schematic diagram of 2D axis symmetry DS furnace system. It consists of a silicon nitride ($Si_3N_4$) coated silica crucible, graphite retort, argon gas tube, graphite heater and graphite insulations. $Si_3N_4$ is used to avoid the diffusion of oxygen impurities from the crucible to melt. Argon gas acts as a carrier gas which is used for the purification of the growth system. The argon gas flow is considered a compressible flow [16]. The growth process depends on the heater power and bottom insulation wall opening rate. Heat transfer mainly occurs in the form of conduction, convection and radiation. 2D grids were generated for the radiative, conductive and convective heat transfers. The iterative method is used to solve heat and mass transfer by using the finite volume method.

The insulation wall is opened after the completion of the melting process. Furnace temperature starts to diminish in the form of heat radiation due to opening the insulation wall at bottom. When the temperature decreases, the molten silicon starts to crystallize. In order to control the growth process, the heater power is controlled in the appropriate manner. The melt was considered as incompressible Newtonian fluid. The rate of the bottom insulation opening was controlled properly for controlling heat dissipation at the bottom. The heat energy is emitted in the radiation form due to the opening of bottom insulation. During this process, the crystal starts to grow from bottom to top [17]. The total number of grids is 9400. In this work we have investigated the different AGFR. Case-a is 5 LPM, case-b is 10 LPM, case-c is 15 LPM, case-d is 20 LPM, case-e is 25 LPM and case-f is 30 LPM. The numerical model details of our system

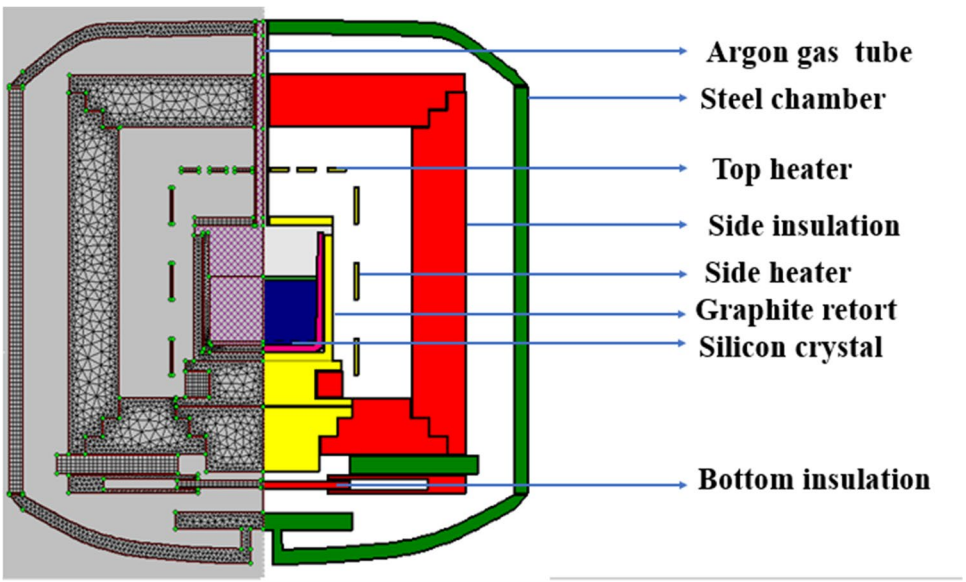


**Fig. 1** Schematic diagram for DS Furnace; left side is grid generated view and right side are furnace materials

are in the reference paper [18]. The material properties are listed in Table 1 for the simulation work.

## 3 Chemical Model

The main difficulty in DS process is to control of the impurity concentration during crystal growth process. The chemical reaction occurs in different stages of the growth process like melting, solidification and cooling process. In this casting process, temperature is raised from the room temperature to above silicon melting point. In that time, crucible reacts with melt, then nitrogen will be formed. Then the silicon melt reacts with the $SiO_2$ crucible, SiO is formed. The SiO gas moves towards the melt-free surface and reacts with the graphite material. Then CO gas is formed. After the CO formation it separates into oxygen and carbon then it is dissolved in the melt. In the melt region if the carbon concentration exceeds the critical value then SiC will be formed. The chemical reactions are as follows:

$$Si_3N_{4\,(S)} = 3Si_{(m)+}\ 4N_{(m)} \tag{1}$$

$$Si_{(m)} + SiO_{2(s)} = 2SiO_{(g)} \tag{2}$$

**Table 1** Physical properties of the material involved in the simulation

| Material | Properties | Values | Units |
|---|---|---|---|
| Argon | Heat conductivity | 0.01 | $W\ m^{-1}\ K^{-1}$ |
| | Heat capacity | 521 | $J\ kg^{-1}\ K^{-1}$ |
| | Dynamic Viscosity | $P(T) = 8.466 \times 10^{-6} + 5.365 \times 10^{-8}$ T-8.682× $10^{-12}\ T^2$ | Pa S |
| Graphite | Heat conductivity | $P(T) = 146.8885–0.17687\ T + 0.000127\ T^2–4.6899 \times 10^{-008}\ T^3 + 6.665 \times 10^{-012}\ T^4$ | $W\ m^{-1}\ K^{-1}$ |
| | Emissivity | 0.8 | |
| | Density | 1950 | $kg\ m^{-3}$ |
| | Heat capacity | 710 | $J\ kg^{-1}\ K^{-1}$ |
| Insulation | Heat conductivity | 0.5 | $W\ m^{-1}\ K^{-1}$ |
| | Emissivity | 0.8 | |
| | Density | 500 | $kg\ m^{-3}$ |
| | Heat capacity | 100 | $J\ kg^{-1}\ K^{-1}$ |
| Quartz | Heat conductivity | 4 | $W\ m^{-1}\ K^{-1}$ |
| | Emissivity | 0.85 | |
| | Heat capacity | 1232 | $J\ kg^{-1}\ K^{-1}$ |
| | Density | 2650 | $kg\ m^{-3}$ |
| Steel | Heat conductivity | 15 | $W\ m^{-1}\ K^{-1}$ |
| | Emissivity | 0.45 | |
| | Heat capacity | 1000 | $J\ kg^{-1}\ K^{-1}$ |
| | Density | 7800 | $kg\ m^{-3}$ |
| Si melt | Heat conductivity | 66.5 | $W\ m^{-1}\ K^{-1}$ |
| | Emissivity | 0.3 | |
| | Density | P(T) = 3194–0.3701 T | $kg\ m^{-3}$ |
| | Melting Temperature | 1685 | K |
| | Surface tension | 0.7835 | $N\ m^{-1}$ |
| | Dynamic viscosity | 0.0008 | Pa S |
| | Heat capacity | 915 | $J\ kg^{-1}\ K^{-1}$ |
| | Wetting angle | 11 | Deg |
| | Latent Heat | 1,800,000 | $J\ kg^{-1}$ |
| Si crystal | Heat conductivity | $P(T) = 110.6122042–0.1507227384\ T + 0.0001093579825\ T^2–4.009416795 \times 10^{-008}\ T^3 + 5.66839358 \times 10^{-012}\ T^4$ | $W\ m^{-1}\ K^{-1}$ |
| | Emissivity | P(T) = 0.9016–0.00026208 T | |
| | Density | 2530 | $kg\ m^{-3}$ |
| | Latent Heat | 1,800,000 | $J\ kg^{-1}$ |
| | Heat capacity | 1000 | $J\ kg^{-1}\ K^{-1}$ |

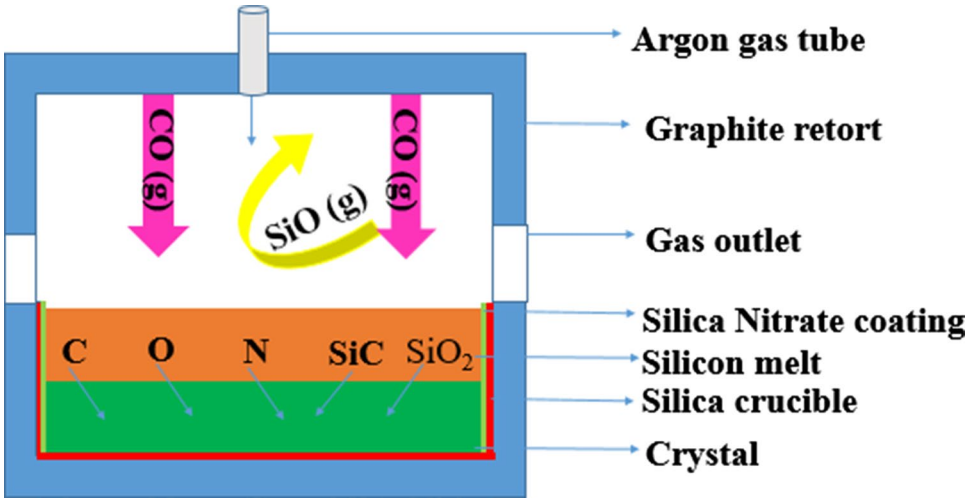


**Fig. 2** Chemical reactions in the DS furnace

$$SiO_{2\ (s)} = Si_{(m)} + 2O_{(m)} \quad (3)$$

$$Si_{(m)} + O_{(m)} = SiO_{(g)} \quad (4)$$

$$SiO_{(g)} + C_{(s)} = CO_{(g)} + Si_{(g)} \quad (5)$$

$$C_{(s)} + SiO_{2\ (s)} = SiO_{(g)} + CO_{(g)} \quad (6)$$

$$CO_{(g)} + 2Si_{(g)} \leftrightarrow SiC_{(s)} + SiO_{(g)} \quad (7)$$

$$Si_{(g)} = Si_{(m)} \quad (8)$$

$$CO_{(g)} = C_{(m)} + O_{(m)} \quad (9)$$

Where (m), (s) and (g) represent the state of melt, solid and gas.

The figure below shows the overall chemical reactions occurring in the DS furnace [16, 18–20] Fig. 2.

## 4 Result and Discussion

Generally, purpose of the argon gas is to carry away the gas from melt-free surface to outlet of the furnace. In the melt-free surface, heat is transferred by the gas convection and radiation. Figure 3 shows the right side of the crucible in the melt-free surface region which explains the argon gas flow

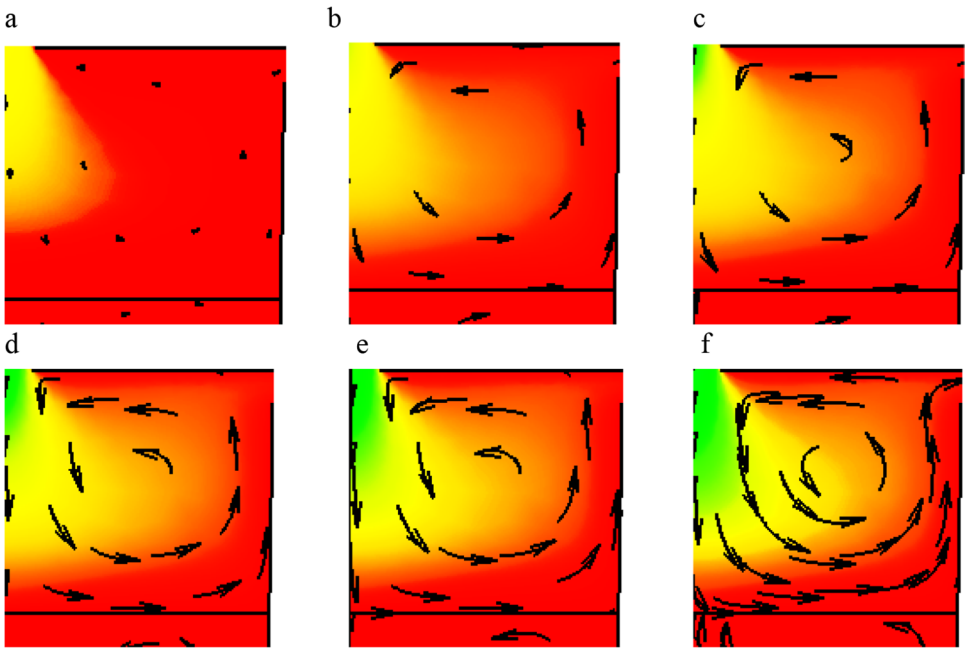


**Fig. 3** Argon gas distribution above melt-free surface. **a**, **b**, **c**, **d**, **e** and **f** correspond to the case-a, case-b, case-c, case-d, case-e and case-f

pattern and influence of argon gas with different flow rate. In the melt-free surface, vector magnitude is varied due to the argon gas flow rate (AGFR). There is no vortex formation in the case-a. After the increment of AGFR velocity, vortex is formed. Thermodynamically, heat convection and radiation move from hot end to cold end. So, vortex is formed in the melt-free surface. Vortexes are formed near the centre of the melt-free surface because argon gas is inserted in the middle zone of the DS furnace. Length of the arrow mark represents the magnitude of argon gas flow velocity. This explains the influence of AGFR. This phenomenon is in agreement with reported results [2]. Higher AGFR affects the temperature distribution of the melt-free surface which is shown in Fig. 4.

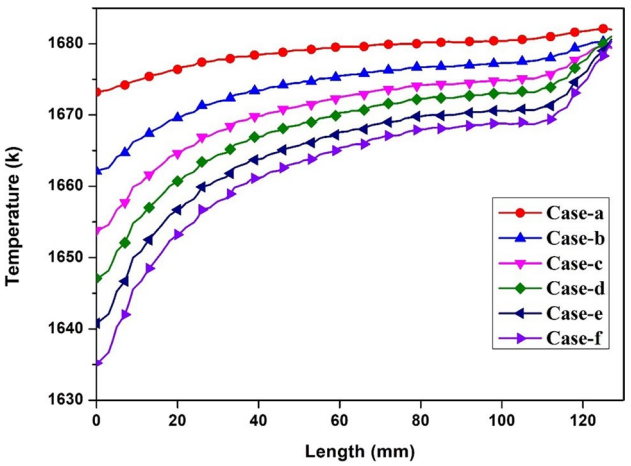


**Fig. 4** Temperature distribution in melt-free surface with different AGFR at 50% grown mc-Si ingot

Figure 4 shows the temperature distribution of right side of the melt-free surface in the crucible. It explains the gas convection of heat transfer related to the temperature distribution pattern. The results show the impact of the AGFR in the melt-free surface after the 50% crystallization process. In minimum amount of AGFR there is no impact created on temperature distribution in melt-free surface. The increment of AGFR influences the heat transfer in the central region of the melt-free surface. The gas distribution will decide the temperature gradient in the melt-free surface. Temperature near the gas outlet is equal for all the AGFR. Temperature variation in the case-a to case-f is 1673 to 1635 K at 50% grown ingot. Figures 3 and 4 show the AGFR impact on the melt-free surface and similar results are reported [2].

## 4.1 Melt Flow Analysis

Figures 5 and 6 show the melt flow velocity at 25% and 50% of solidification fraction. During the mc-Si ingot casting process, heat is transferred from the melt by heat conduction, convection and radiation process. In both 25% and 50% of solidification fraction, heat convection occurs in the clockwise direction. Above the case-c, the direction of the flow pattern varies from clockwise to counter-clockwise pattern. This will help to eject the impurity from the crystal.

At 25% of solidification fraction in case-e secondary vortex is formed. In Fig. 6. case-f the secondary vortex is

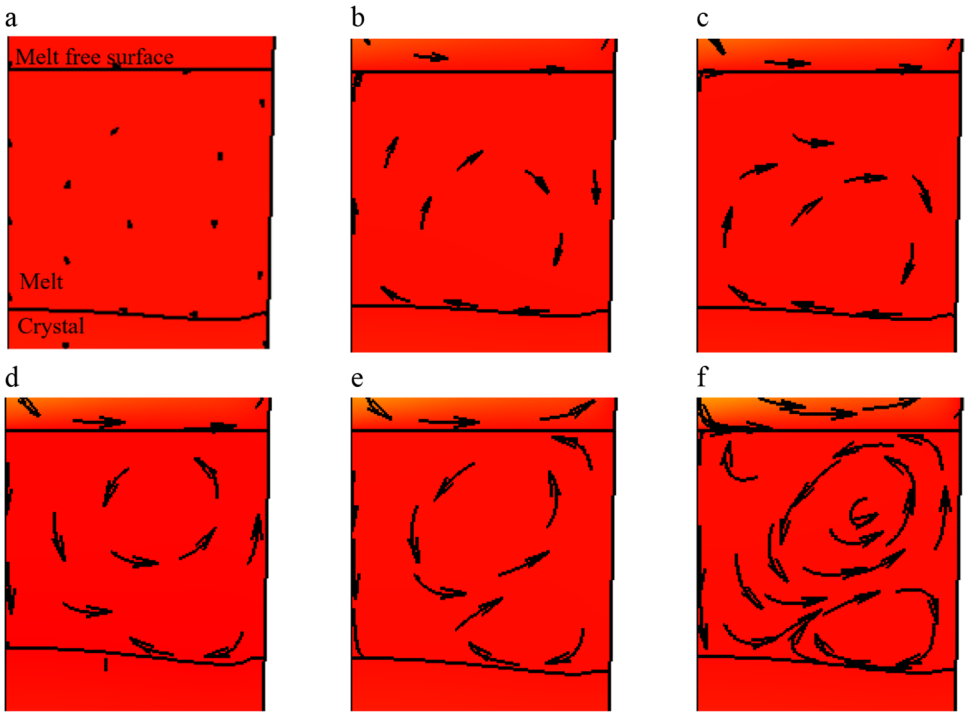


**Fig. 5** Velocity of the melt after 25% growth of mc-Si ingot **a**, **b**, **c**, **d**, **e** and **f** correspond to the case-a, case-b, case-c, case-d, case-e and case-f

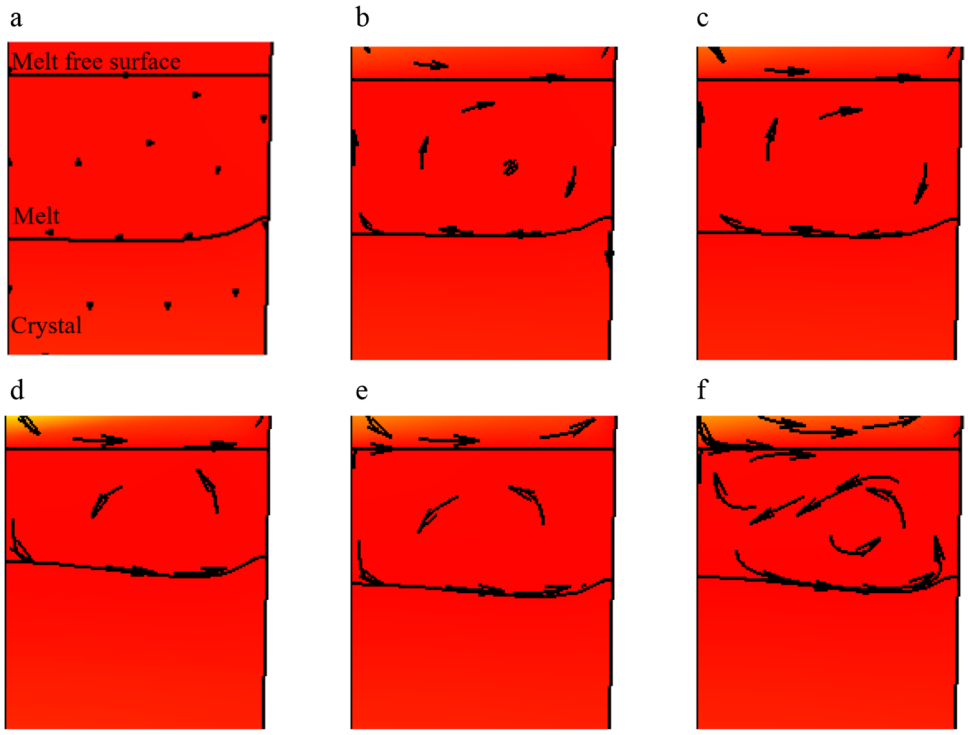


**Fig. 6** Velocity of the melt after 50% growth of mc-Si ingot **a**, **b**, **c**, **d**, **e** and **f** corresponding to the case-a, case-b, case-c, case-d, case-e and case-f

formed due to higher AGFR. This type vortex has reduced the impurity concentration [4].

### 4.2 Oxygen Impurity Concentration Analysis

Silica crucible acts as a source of the oxygen. Crystal and melt act as sink. The interstitial oxygen will improve the mechanical strength of the wafer [20] and it does not affect the minority carrier life time [21, 22]. In boron doped mc-Si, excess of oxygen induces the oxygen boron (O-B) complex in order to form LID effect in the solar cell which reduces the efficiency. It also affects the mechanical strength of the wafer [23]. The melt flow and gas flow strongly affect the oxygen concentration and distribution. The LID effect can be avoided by controlling the oxygen concentration below 1.5E17 atoms/cm$^3$ in the crystal [13].

Figure 7 shows oxygen concentration. The distribution of the oxygen varies inside the melt due to the different AGFR. Most of the oxygen is dissolved into the melt during the melting process, then it forms SiO gas. Oxygen concentration is high near to the crucible wall due to the dissolution of oxygen from the crucible wall. The oxygen concentration in the top of the melt is less compared to the bottom. In case-a, the oxygen concentration inside the melt is7.4E17 atoms/cm$^3$ at the initial stage. But this higher value is in a small area. When the AGFR increases the oxygen concentration decreases. The maximum amount of oxygen concentration is found in case-a to case-d as seen in the Fig. 7 left side. In case-a to case-d the AGFR are not sufficient to carry more SiO gas which enhances the chemical reactions. In case-e and case-f, the oxygen concentration range is from 7E16 to 2.0E17atoms/cm$^3$. In the Fig. 7 right side shows the 50% melt portion. In case-a and case-f, the oxygen concentration range is from 4.0E16 to 7.2E17atoms/cm$^3$. In all cases the upper part of the melt has a low oxygen concentration compared to the lower part due to the argon gas flow. In the upper part of the melt which is nearby the melt-free surface, the SiO gas is captured easily. In CZ process the main motto is to control the oxygen concentration in the melt within the solubility limit of 2-3E18 atoms/cm$^3$ to avoid the dislocation generation from the $SiO_2$ [24]. Oxygen concentration in the growing ingot is directly proportional to the oxygen which is diffused from the silica crucible and reacts with the melt. The reaction is temperature dependent [25].

In Fig. 8 left side indicates the 25% grown mc-Si ingot and right side is 50% grown ingot. The oxygen concentration is varied from the melt to crystal because some of the oxygen forms into SiO gas. In Fig. 7 left side case-a has high oxygen concentration compared to other cases. Near the crucible wall it is 7.0E17 atoms/cm$^3$ and remaining portion it is below 5.3E17 atoms/cm$^3$. The more amount of oxygen concentration is dissolved from the crucible wall into the melt and it gets into the crystal [20]. Convective flow transport is very important to control the oxygen concentration in the crystal because the oxygen atoms are transported into the melt via convection flow. If oxygen concentration is above the critical value inside the crystal, it induces the LID effect [14]. High AGFR has reduced the

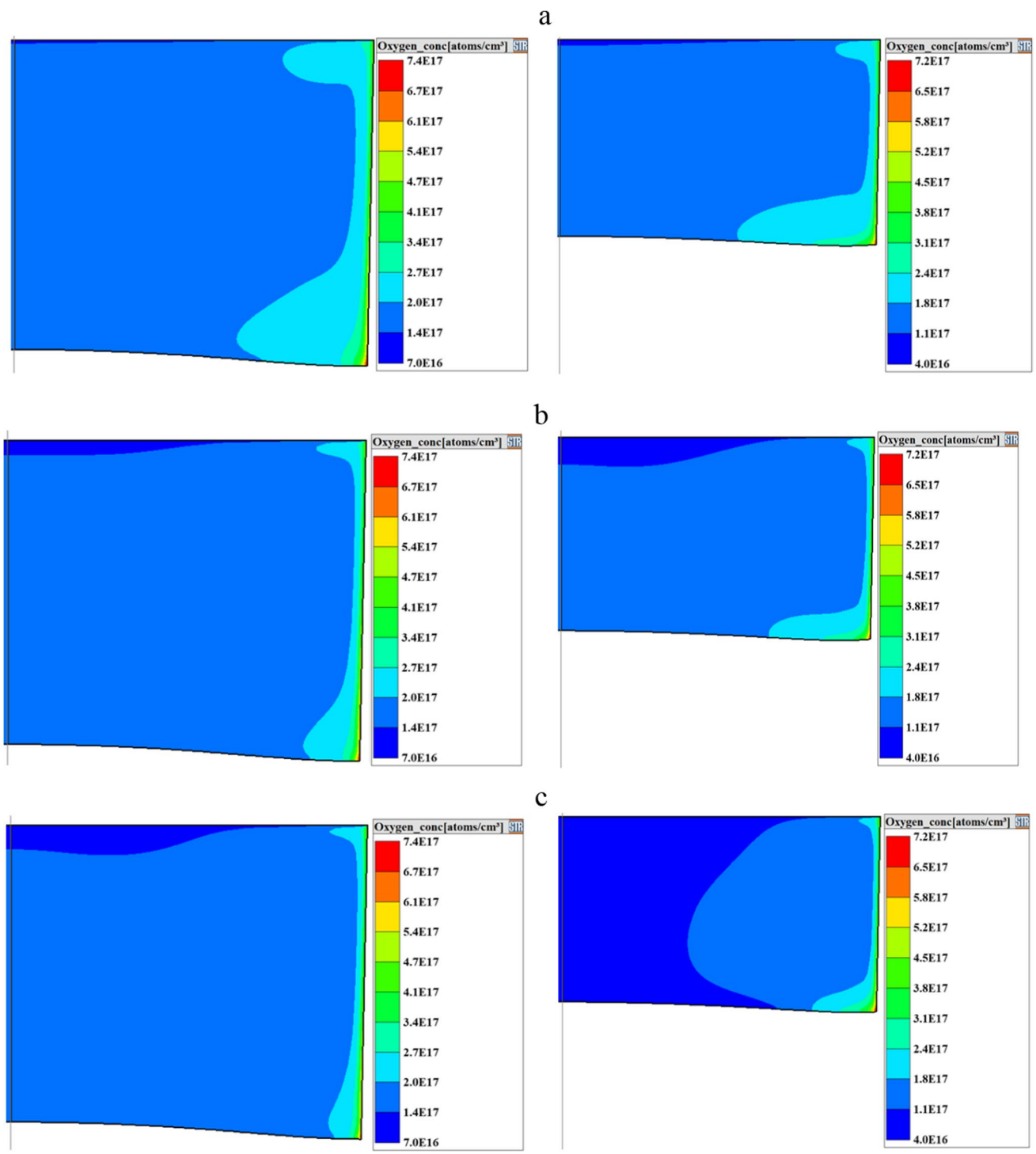


**Fig. 7** Oxygen concentration, at 75% melt (left) and Oxygen concentration, at 50% melt (right). **a**, **b**, **c**, **d**, **e** and **f** correspond to the case-a, case-b, case-c, case-d, case-e and case-f

oxygen concentration in the grown ingot. Case-a to case-c, the oxygen concentration level in the ingot is above the critical level. After the case-c, the oxygen concentration level is less compared to the critical value. In the Fig. 8 right side shows the crystal portion after 50% solidification fraction. The oxygen concentration of case-a to case-c is in the range of 8.5E16 to 7.5E17 atoms /cm3. It easily enhances the LID effect and SiO2 formation. The minimum amount of AGFR is not enough to reduce the oxygen concentration. Case-d to case-f have better result and the

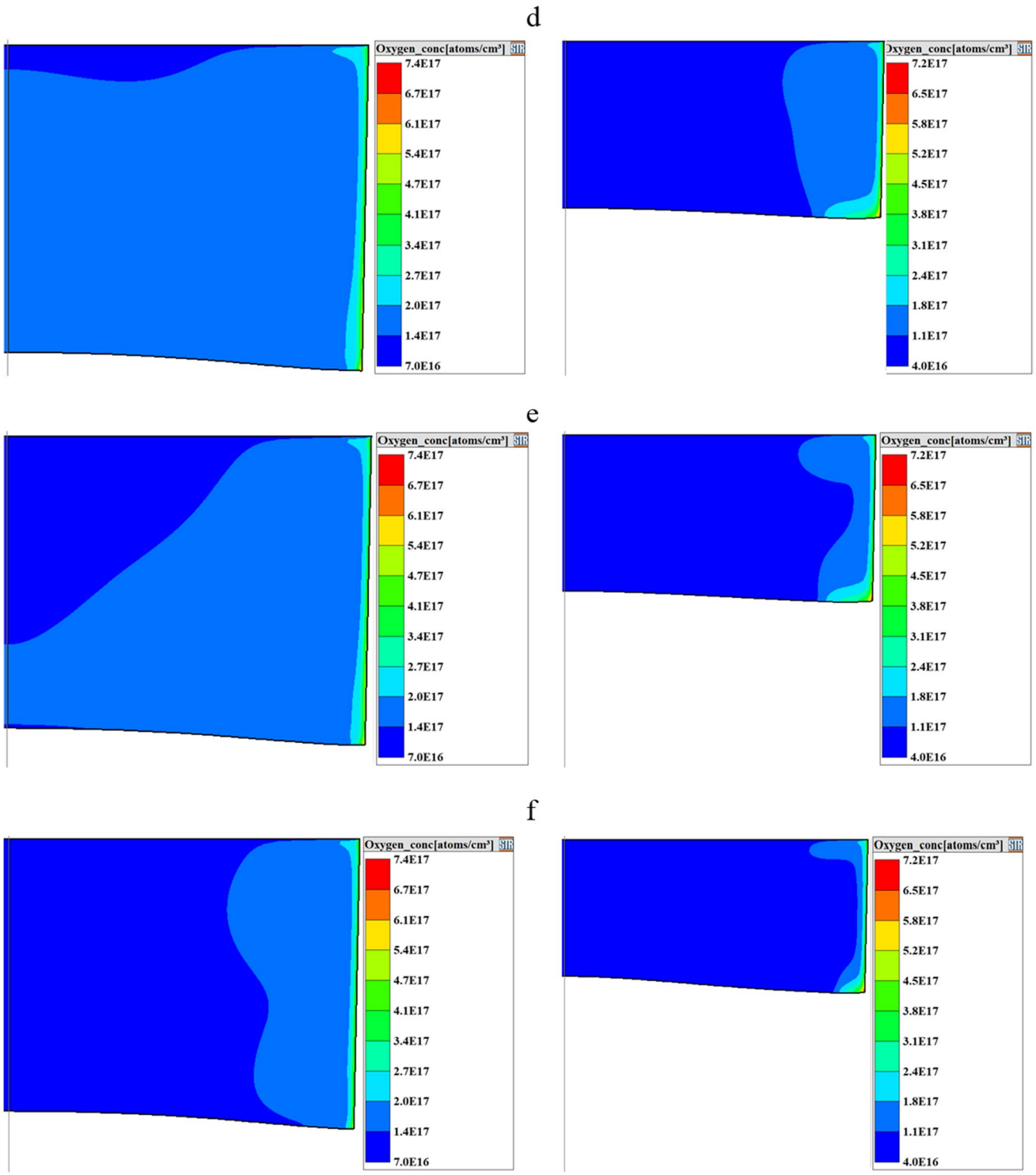


**Fig. 7** (continued)

oxygen concentration level is in the range of 2.8E17 to 8.5E16 atoms /cm3.

Figure 9 shows the fully grown mc-Si ingot. Minimum amount of AGFR slightly affects the oxygen impurity distribution. Figure 9 case-a to case-c, have higher oxygen concentration inside the ingot. Such types of ingots are enhancing more LID effect, $SiO_2$ formation and reduces the minority carrier lifetime. Minimum AGFR is not sufficient to grow better quality mc-Si ingot. After the case-c, the oxygen concentration is reducing gradually due to higher

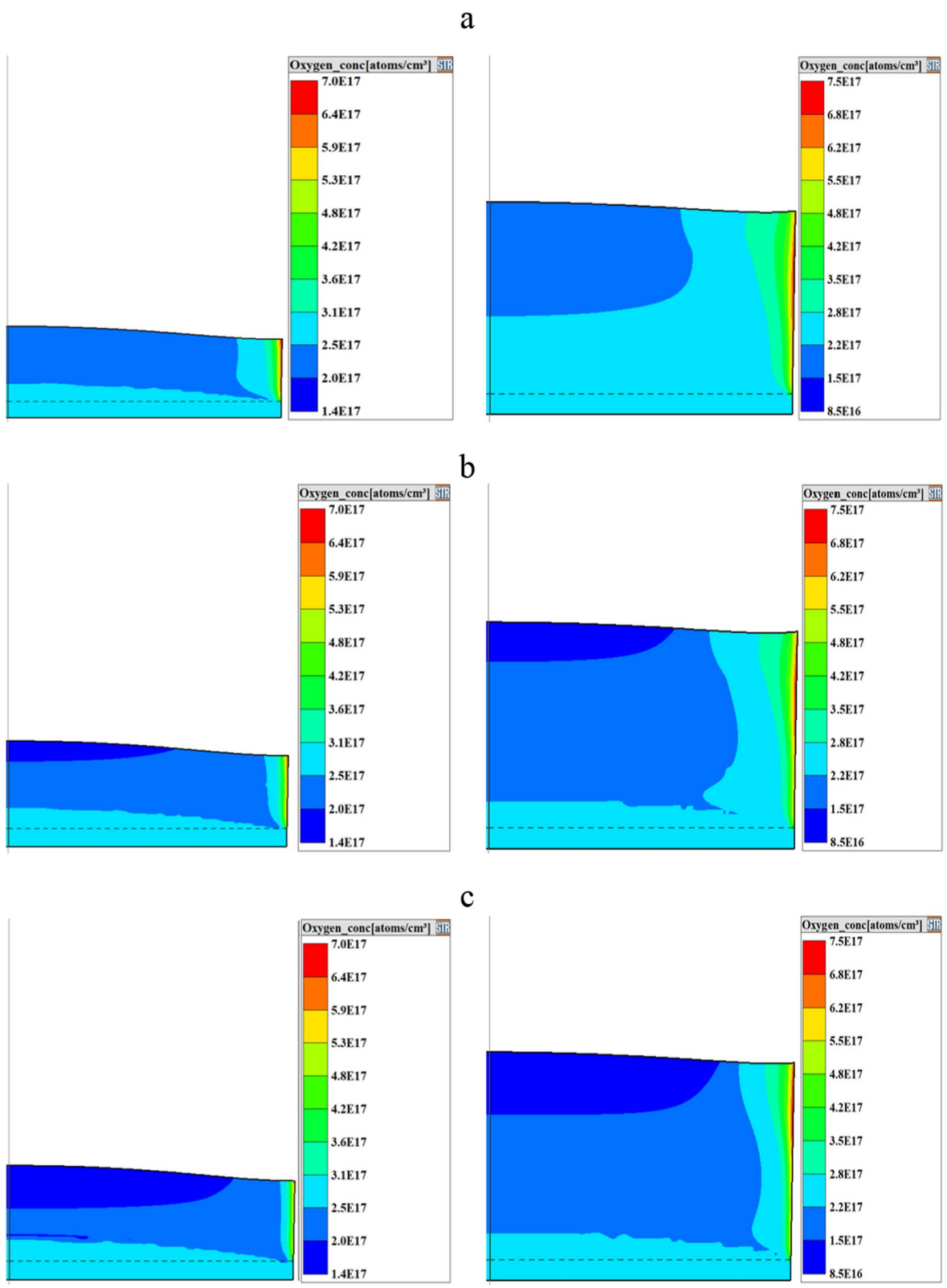


**Fig. 8** Oxygen concentration at 25% grown ingot (left) and Oxygen concentration at 50% grown ingot (right). **a**, **b**, **c**, **d**, **e** and **f** correspond to the case-a, case-b, case-c, case-d, case-e and case-f

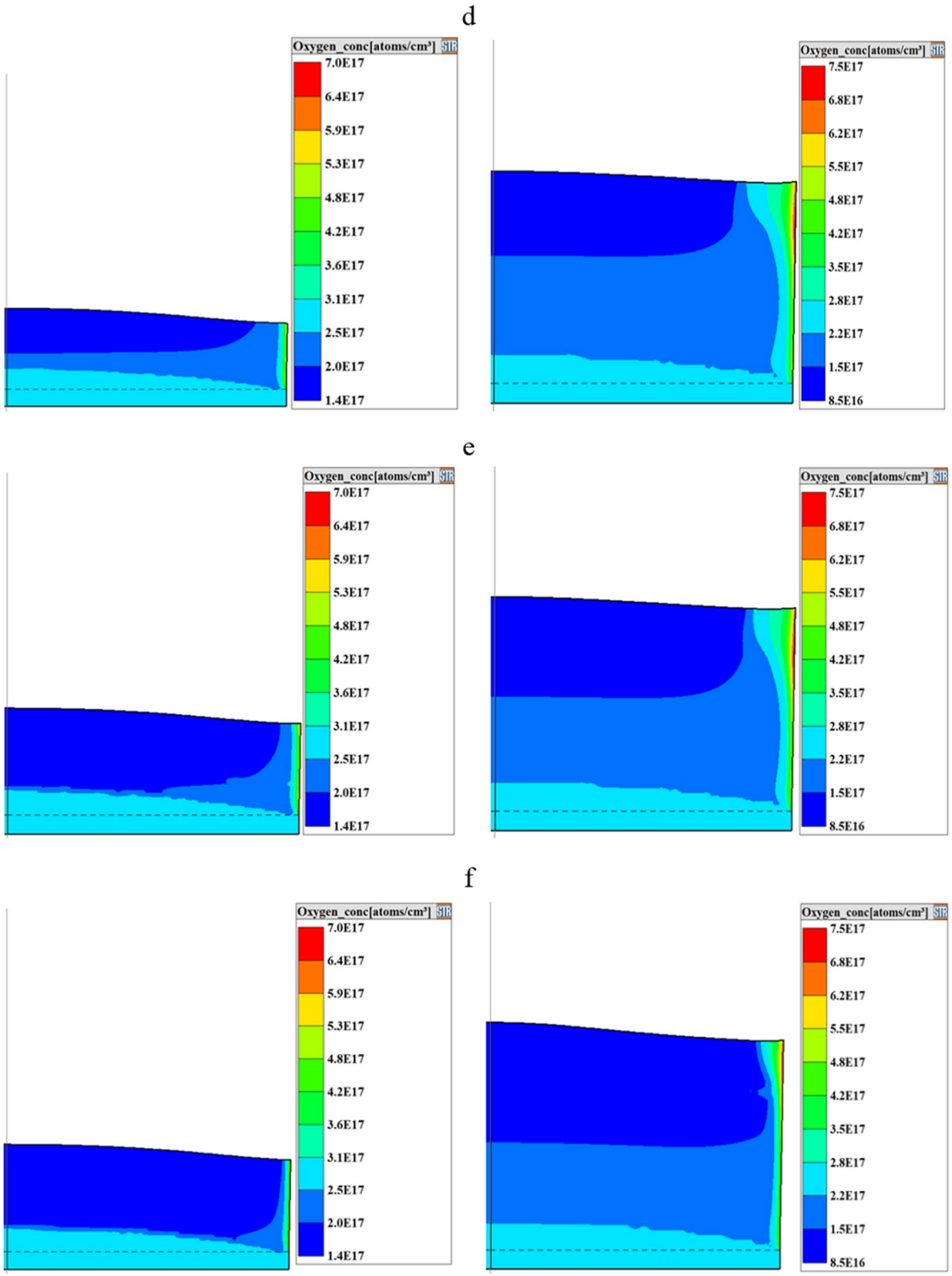


**Fig. 8** (continued)

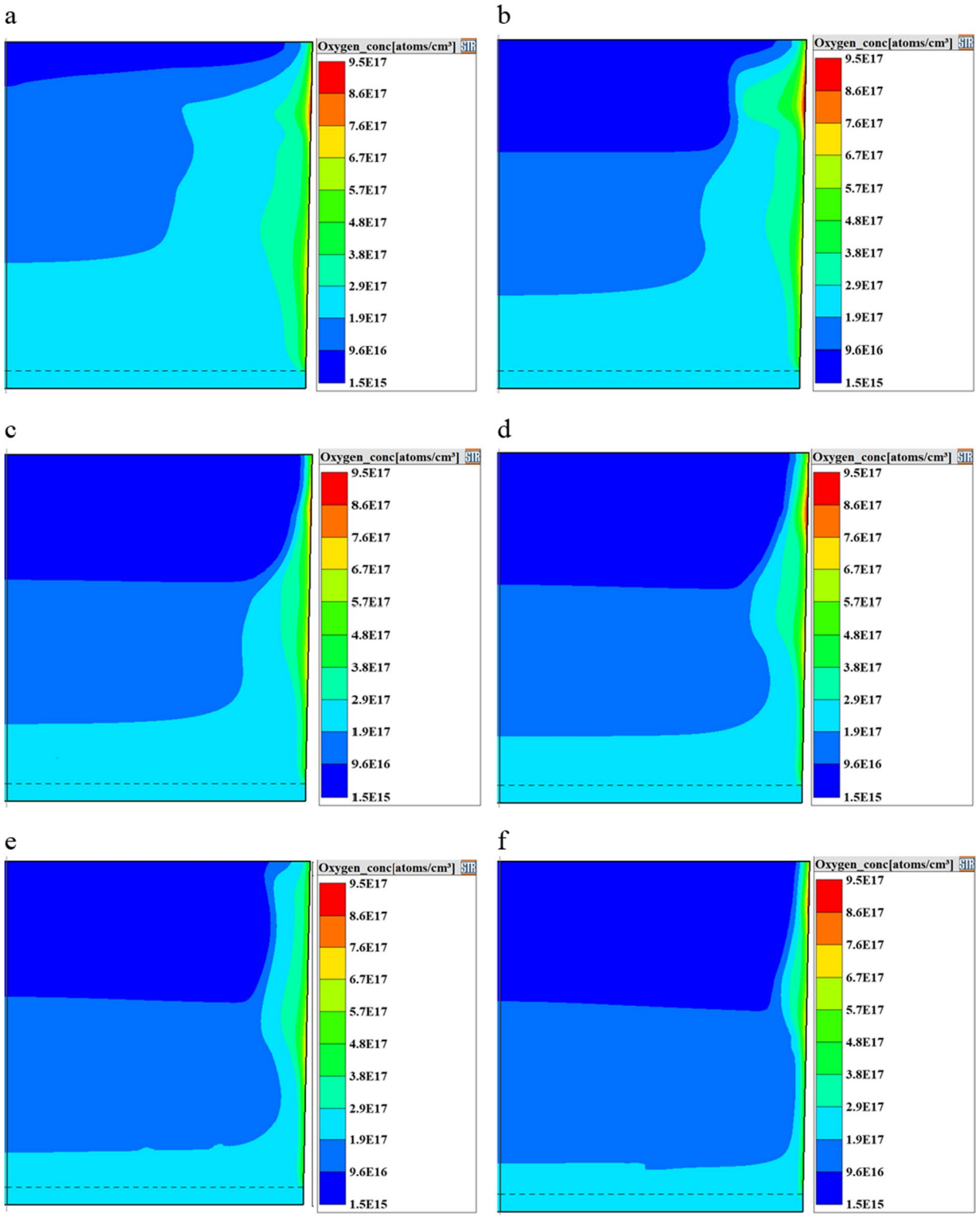


**Fig. 9** Oxygen concentration, after growth of 100% of mc-Si ingot. **a**, **b**, **c**, **d**, **e** and **f** correspond to the case-a, case-b, case-c, case-d, case-e and case-f

AGFR. The oxygen concentration of case-e and case-f is below 2.9E17 atoms/cm$^3$. In case-e and case-f the oxygen concentration is less than the critical value of the grown ingot. In both cases very small portion is above the critical

value which is negligible. In electronic application CZ wafers are used with the oxygen concentration of 3-9E17 atoms/cm$^3$ [26]. From case-e, the gas flow rate starts to reduce the LID effect which denotes that the case-e is better in oxygen concentration point of view.

### 4.3 SiO Gas Analysis

The SiO gas formation rate depends on the different parameters like the temperature distribution, melt flow rate and argon gas flow rate.

The transport of the oxygen atoms into the melt is through diffusion and convective flow which reacts with silicon to form SiO gas. Then the SiO gas moves from melt to melt-free surface due to density variation. In Fig. 10. case-a has higher SiO gas in the melt-free surface because of the low AGFR. By increasing AGFR, the SiO gas concentration is reduced in the melt-free surface during the growth process. In case-a, the SiO concentration in the melt-free surface is distributed homogeneously. By increasing the argon gas flow, the SiO concentration is varied due to the elimination of SiO gas nearby the melt. The SiO concentration in the melt-free surface varies from 0 to 6.9E2 ppma at 25% grown ingot and 0 to 5.0E2 ppma at 50% grown ingot. The maximum value of the SiO gas concentration is present nearby the melt-free surface.

### 4.4 Carbon Impurity Concentration Analysis

Carbon and related defects play an important role in the efficiency of solar cell. Carbon impurity affects the dislocation density in the ingot. The excess of carbon occupies the silicon crystal as substitutional or interstitial sites due to point defects. If the carbon exists as the substitutional in a silicon atom, then it is electrically inactive. If the carbon exists as the interstitial in silicon atom, then it is electrically active and also affects the dislocation density [27–29]. The carbon impurities are originating from the melting stage and growth stage of the casting process.

The Fig. 11 shows the 75% and 50% melt portion. The concentration of carbon impurity in melt varies from top to bottom position. The high carbon concentration value is in the top and minimum amount is in the bottom of the melt. High carbon concentration appears in between the edge of the melt and top of the crucible wall. Carbon concentration in case-a to case-f is 3.0e17 to 4.0E17atoms/cm$^3$ as shown in the Fig. 11. In Fig. 11 case-a to case-d, the carbon concentration is higher than case-e and case-f which enhances the oxygen precipitation in the melt [13]. By increasing the AGFR, it will reduce the carbon concentration which results in the reduction of oxygen precipitation in the melt. It is in Fig. 7. In Fig. 11 right side, the carbon concentration varies from the 3.9E17 to 5.6E17 atoms/cm$^3$. Carbon concentration becomes less from case-e due to the increment of the AGFR both at 75% and 50% melt. SiC formation is avoided as carbon concentration is less than the critical value.

Figure 12 left and right sides are showing the 25% and 50% of the grown mc-Si ingot. In the grown ingot carbon impurities are high in the top of the crystal due to its segregation coefficient. The CO gas was absorbed in the top of the melt after the convection or diffusivity and it gets segregated to the crystal. By increasing the AGFR the CO gas back diffusion is decreased and the segregation of the carbon in crystal is also reduced. The carbon concentration of 25% and 50% grown ingot are corresponding to 1.5E16 to 2.4E16 atoms/cm$^3$ and 1.5E16 to 3.5E16 atoms/cm$^3$ respectively.

Figure 13 shows the carbon concentration on fully grown mc-Si ingot. The case-a and case-b have higher value of carbon concentration in the grown ingot. From case-b onwards the carbon concentration is suppressed due to the increase in AGFR. Analysing all cases carbon concentration is in the range of 1.5E16 to 2.2E17 atoms/ cm$^3$. From case-c the carbon impurity is less than 5.6E16 atoms/cm$^3$. When we consider the carbon concentration from case-d onwards there is good quality mc-Si ingot.

### 4.5 CO Gas Analysis

Figure 14 shows the CO gas in the melt-free surface with different gas flow rate at 25% and 50% grown crystal.

The CO formation and back diffusion take place at the triple point which results in higher oxygen concentration in the melt [16, 25]. The concentration of the CO gas is increasing from bottom to top of the melt-free surface. The CO gas concentration nearby the graphite material is high due to chemical reaction which happens due to the SiO gas. CO gas enters into the melt by back diffusion or convection during the solidification process. The CO concentration in the melt-free surface varies from 0 to1.3E2 ppma at 25% grown ingot and 0 to 9.5E1 ppma at 50% grown ingot CO concentration decreases with respect to the increment of AGFR. In the case-a CO gas concentration has higher value than the other cases. This indirectly represents that the argon gas is carrying out the CO gas. At higher flow rate CO gas concentration is reduced. From case-c, carbon concentration at grown mc-Si ingot is below the critical value for SiC formation.

## 5 Experimental Procedure

In the DS process initially feedstock is loaded in the quartz crucible and it is heated above the melting point. After the melting, the temperature is maintained a few

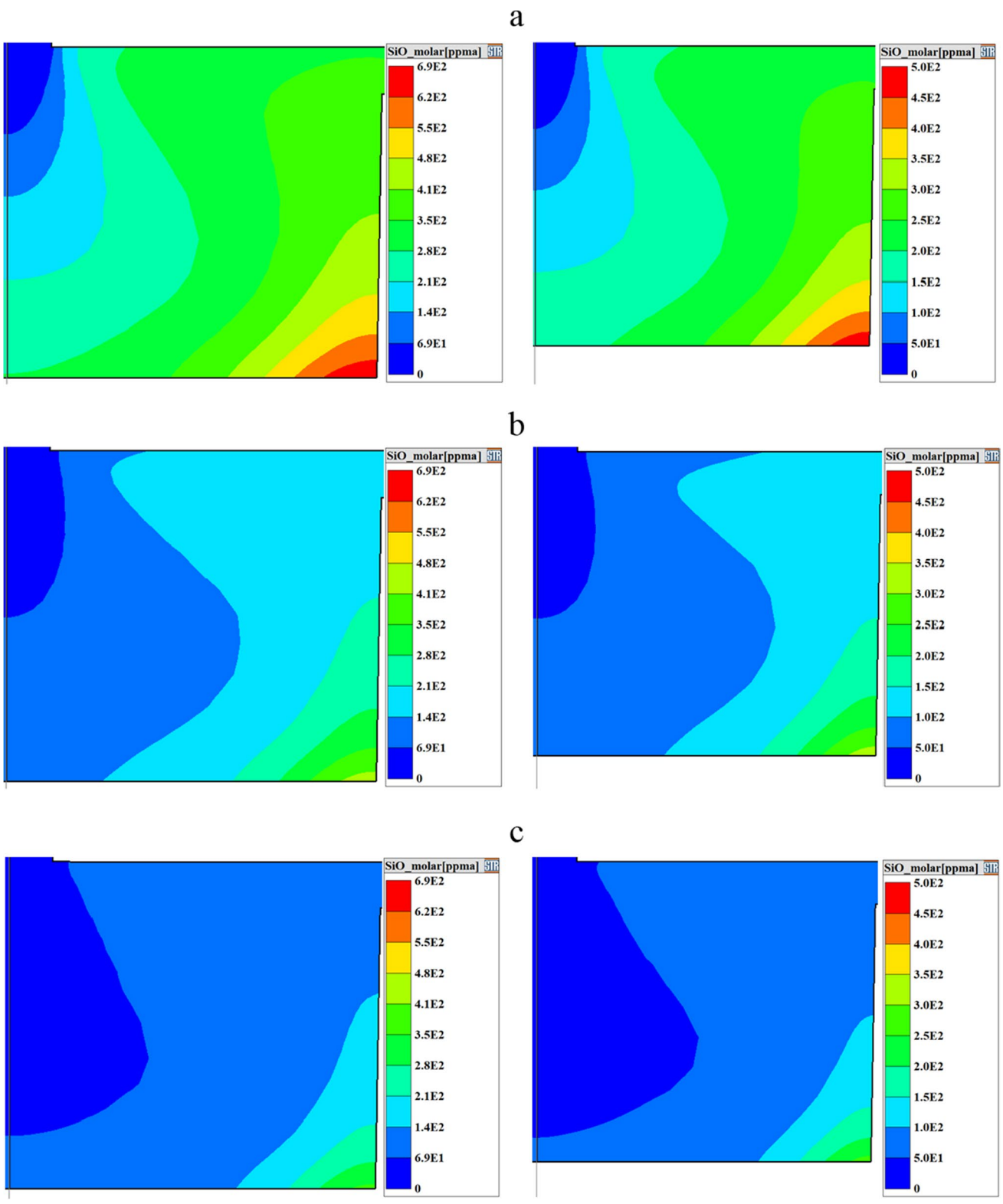


**Fig. 10** SiO gas concentration in melt-free surface. Left side is 25% grown mc-Si ingot and right side is 50% grown mc-Si ingot. **a**, **b**, **c**, **d**, **e** and **f** correspond to the case-a, case-b, case-c, case-d, case-e and case-f

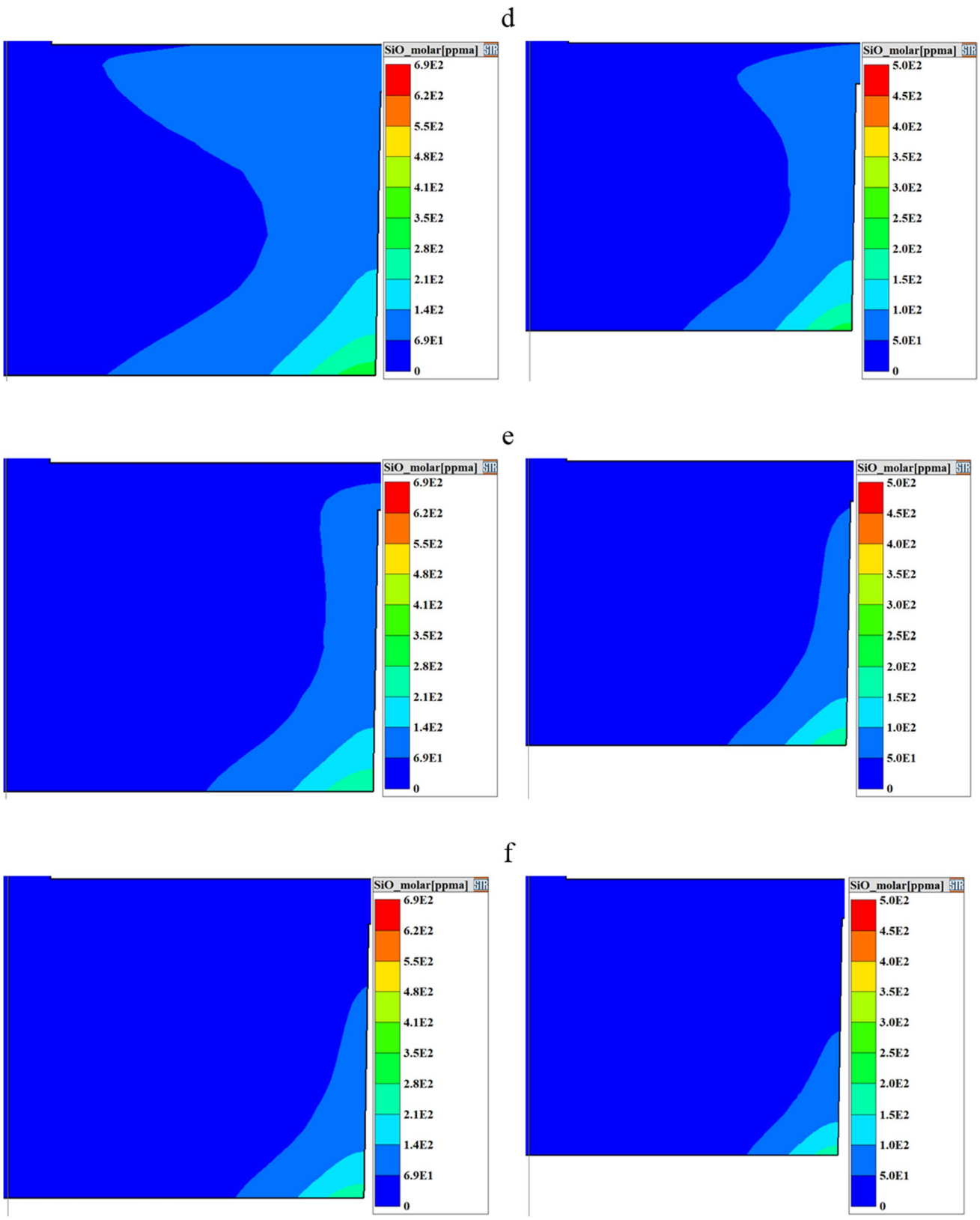


**Fig. 10** (continued)

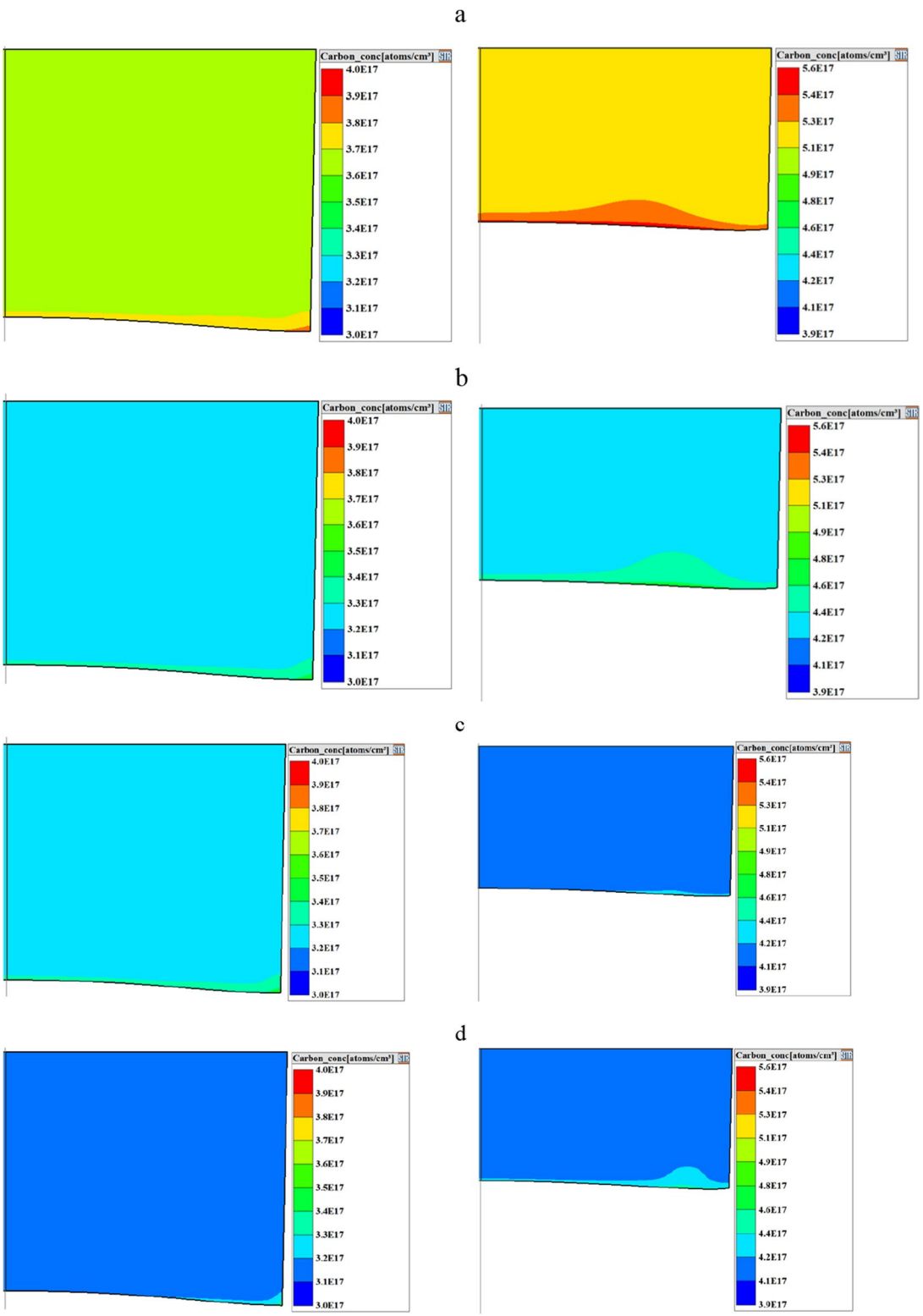


**Fig. 11** Carbon concentration, at 75% melt (left) and carbon concentration, at 50% melt (right). **a**, **b**, **c**, **d**, **e** and **f** correspond to the case-a, case-b, case-c, case-d, case-e and case-f

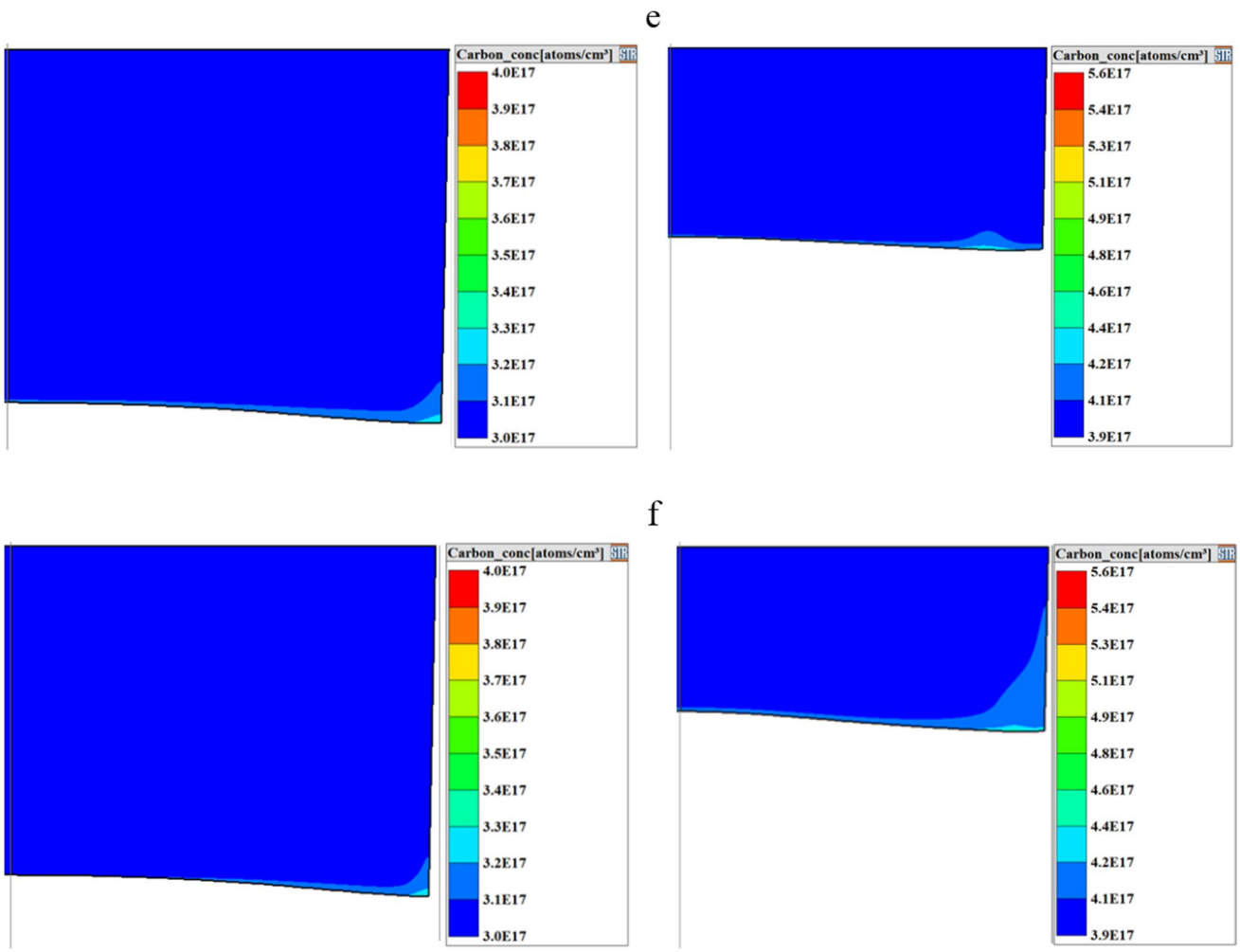


**Fig. 11** (continued)

hours at above the silicon melting temperature for uniform melting than is solidified with controlled cooling. Based on the numerical simulation results, the 25 LPM AGFR was used to grow mc-Si ingot with a weight of 15 kg.

Figure 15 shows the as grown mc-Si ingot and DS system. After the DS process, the ingot is cut. The samples are collected from the corner and centre of the ingot. Sample position are shown in Fig. 16. The wafer was taken from the top, middle and bottom of the corner and the centre of the brick. The collected wafer dimension is 15*15*2 mm and compared with the impurity concentration by FTIR spectrum.

## 5.1 FTIR Analysis

The sliced wafer carbon and oxygen concentrations are measured by using the FTIR analysis for the corner and centre of the ingot particularly the top, middle and bottom. Due to the segregation coefficient, the concentration of carbon and oxygen in the ingot varies. The peak at 608 cm-1 corresponds to carbon, and the peak around 1112 cm-1 corresponds to oxygen in the interstitial spaces. Si-C and Si-Si stretching vibrational modes are responsible for the small band around 600 cm-1. Si-O stretching mode symmetric and asymmetric stretching accounted for the bands present at 1050 and 1110 cm-1. Variations in carbon and oxygen concentrations can be seen in the obtained spectra. The below equation is used to calculate the carbon and oxygen concentration in wafers.

$$N = C \times 2.303 \left(A_p - A_b/d\right) \tag{10}$$

C Conversion Coefficient

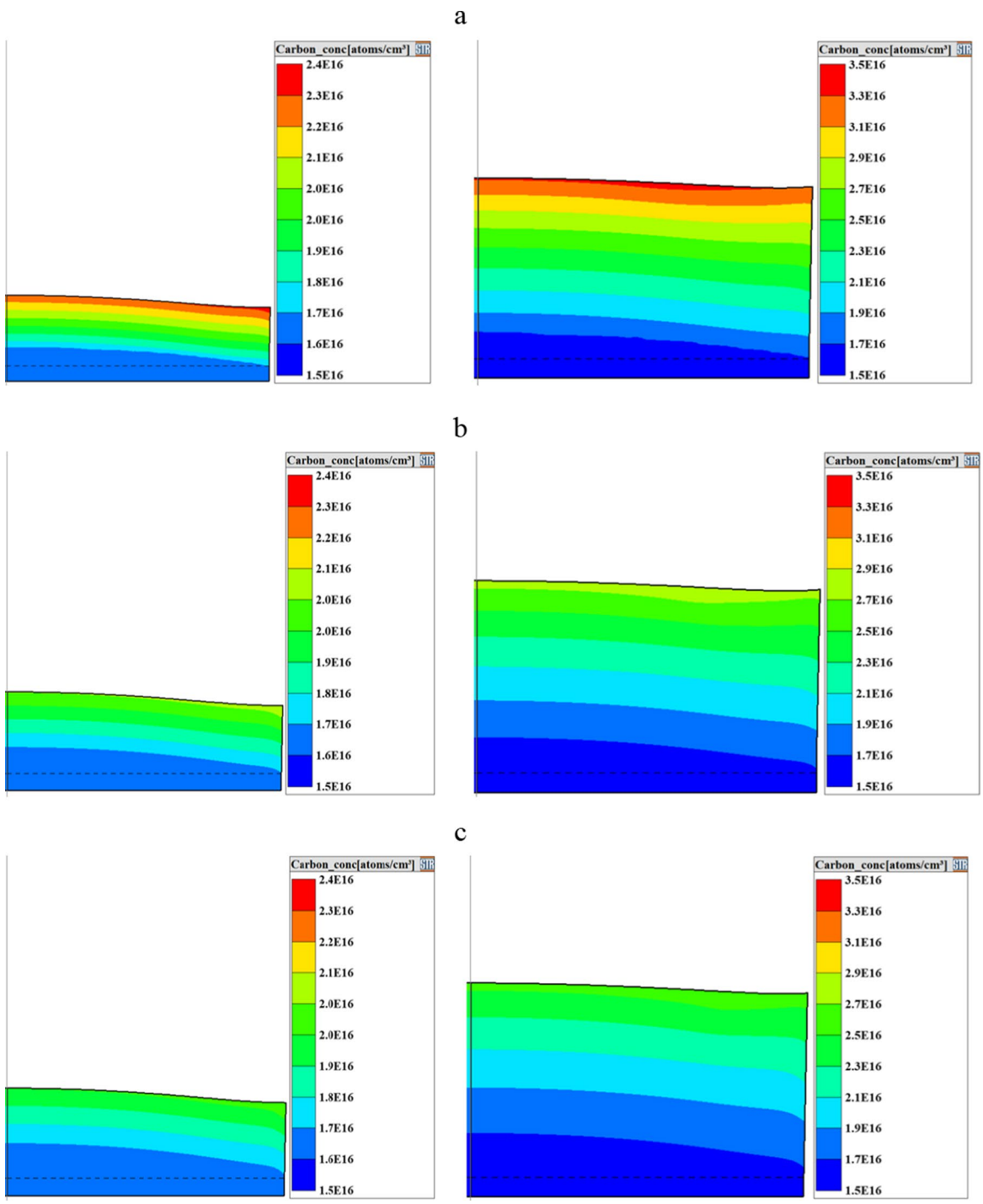


**Fig. 12** Carbon concentration at 25% grown ingot (left) and carbon concentration at 50% grown ingot (right). **a**, **b**, **c**, **d**, **e** and **f** correspond to the case-a, case-b, case-c, case-d, case-e and case-f

$A_p$ Obtained Absorbance Value

$A_b$ Baseline Absorbance Value

d Thickness of the wafer

Carbon and oxygen has different conversion coefficient. The conversion coefficient of carbon at room temperature

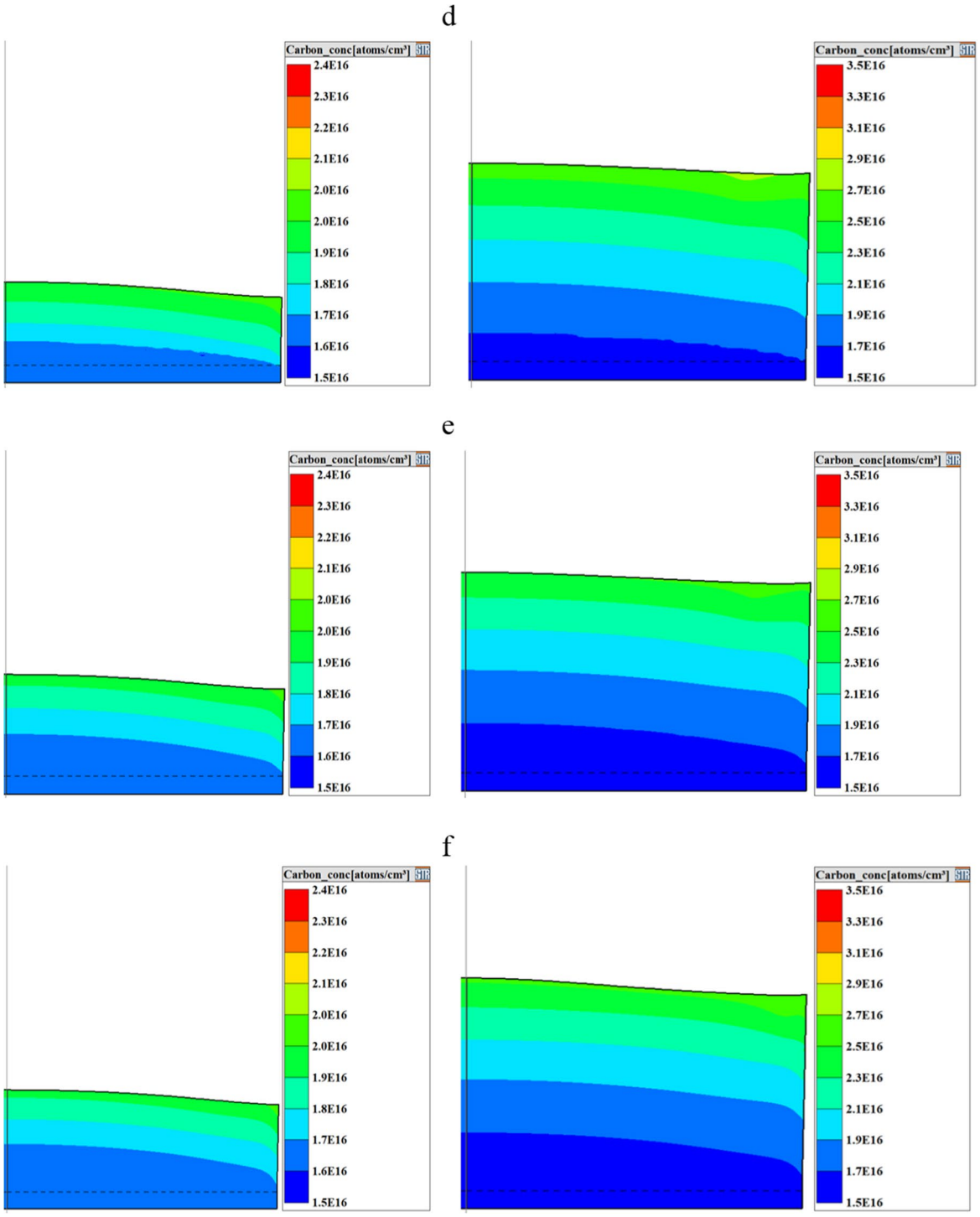


**Fig. 12** (continued)

is 8.2E16 $cm^{-2}$. The conversion coefficient of oxygen at room temperature is 3.1E17$cm^{-2}$ [30].

In Fig. 17 left side is a corner zone of the wafer and the right side is the centre zone of the wafers to obtain the impurity concentration for the grown ingot. The carbon and oxygen concentration values are given in Table 2.

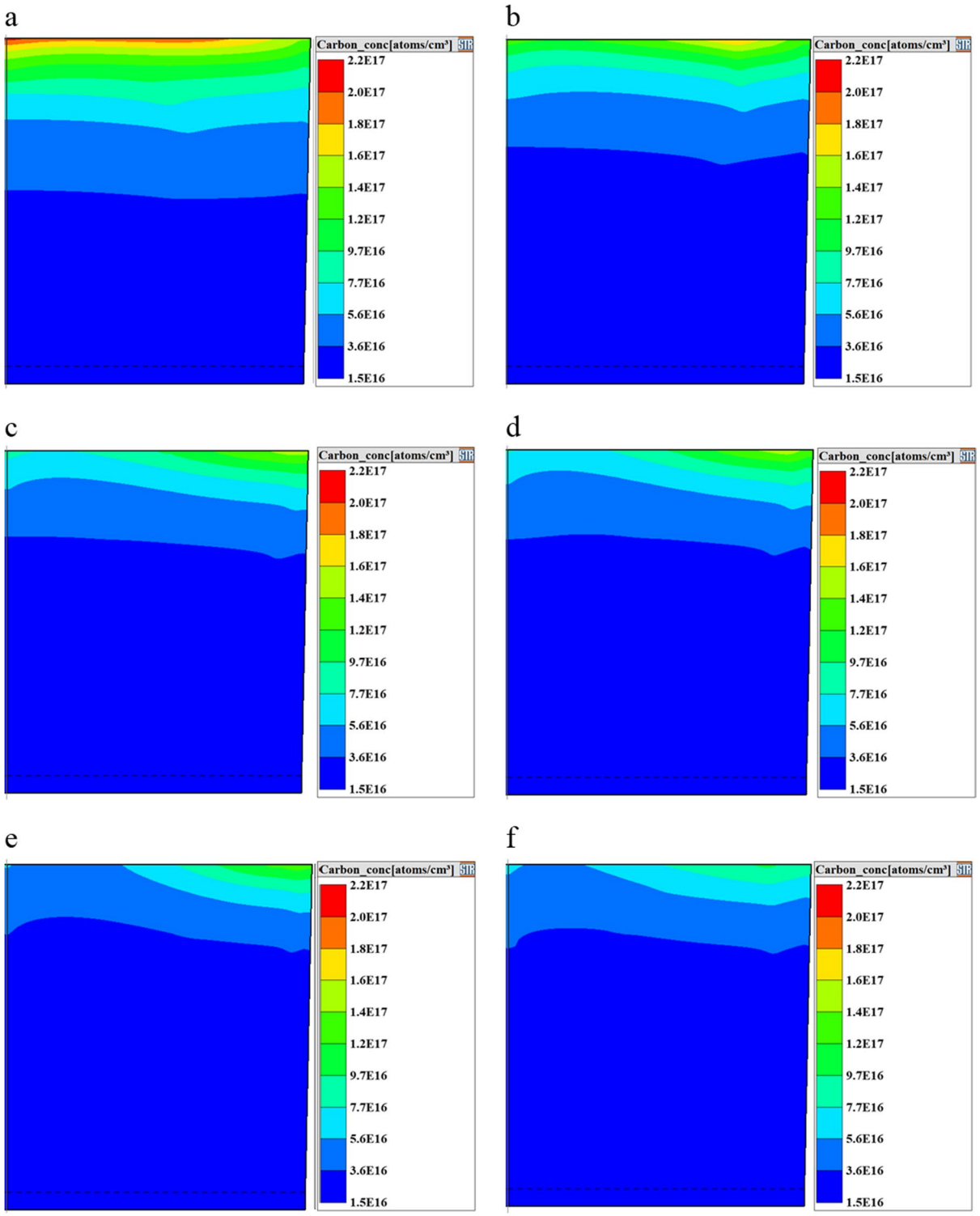


**Fig. 13** Carbon concentration, after growth of 100% of mc-Si ingot. **a**, **b**, **c**, **d**, **e** and **f** correspond to the case-a, case-b, case-c, case-d, case-e and case-f

These results have shown that the corner region of the wafer has a huge amount of impurity concentration compared to the centre region of the ingot. These results are similar to the simulation results.

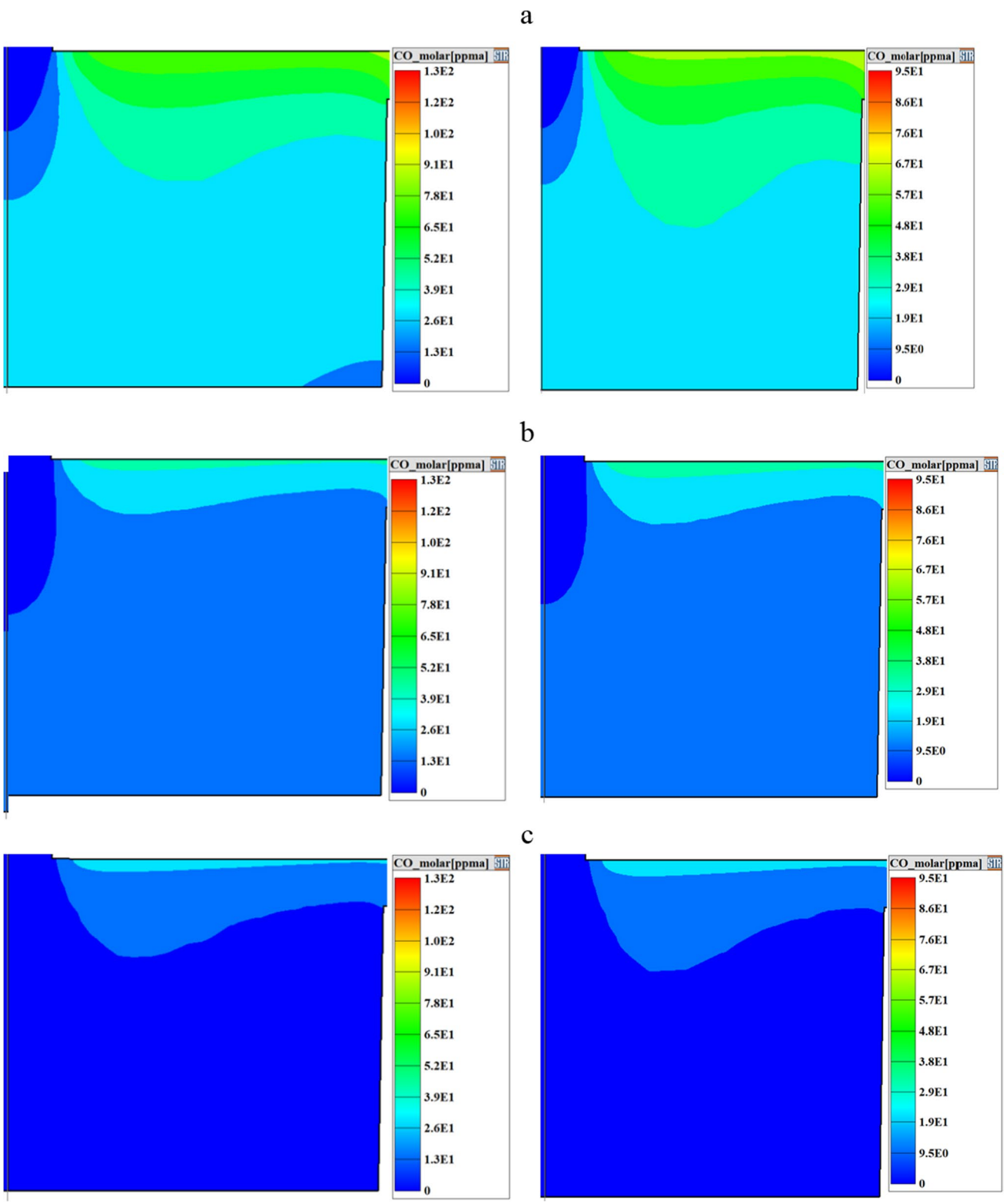


**Fig. 14** CO gas concentration in melt-free surface. Left side is 25% grown mc-Si ingot and right side is 50% grown mc-Si ingot. **a**, **b**, **c**, **d**, **e** and **f** correspond to the case-a, case-b, case-c, case-d, case-e and case-f

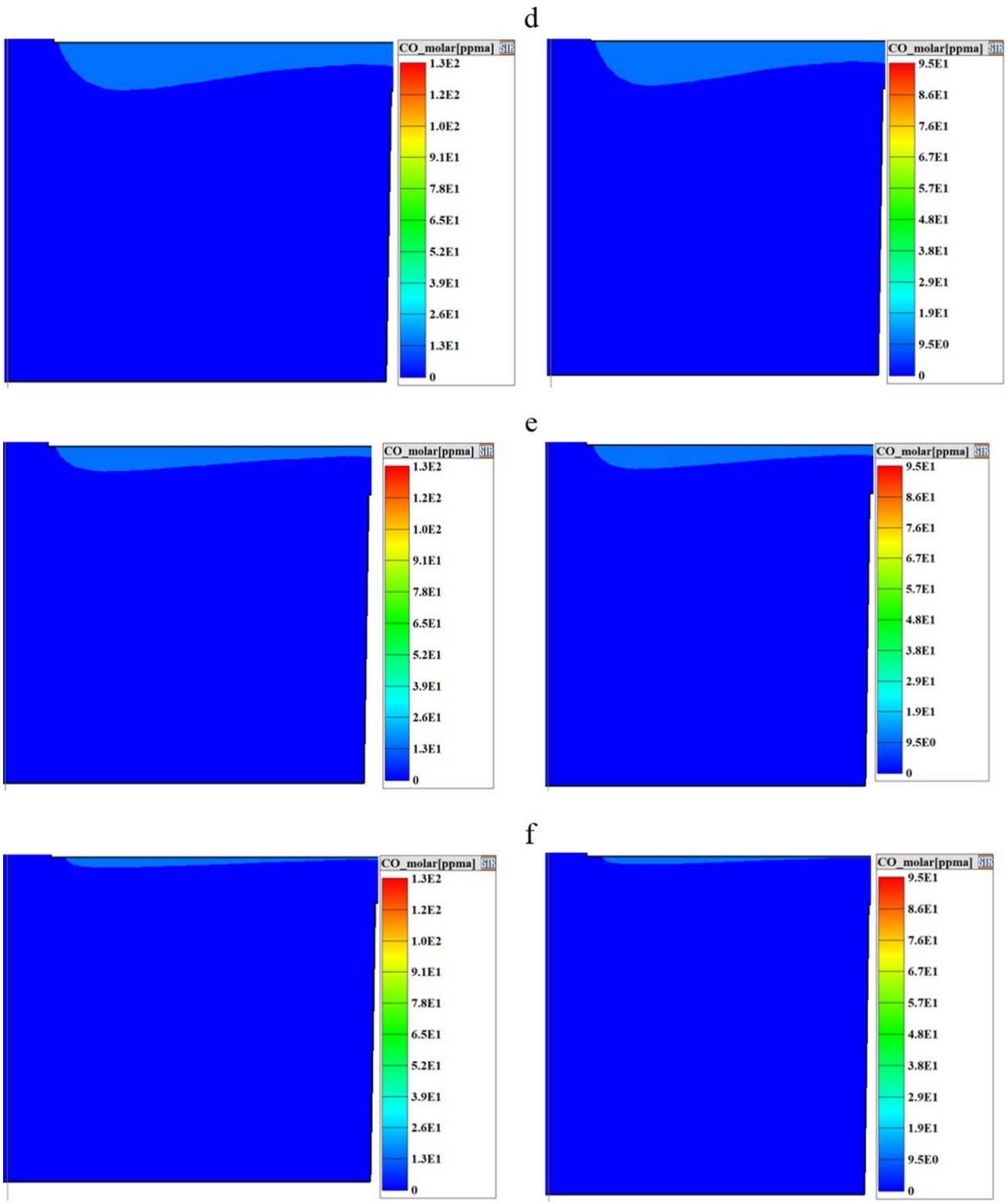


**Fig. 14** (continued)

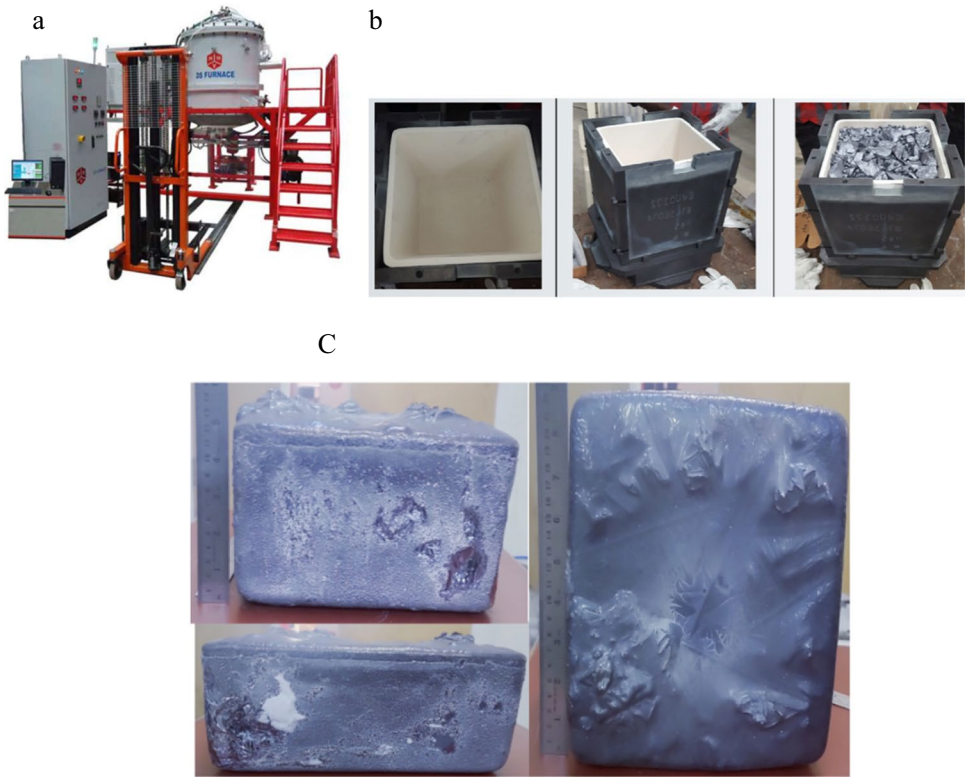


**Fig. 15** DS Furnace experimental setup. **a**. Experimental setup of DS furnace, **b**. Feedstocks loading and **c**. Grown mc-Si ingot

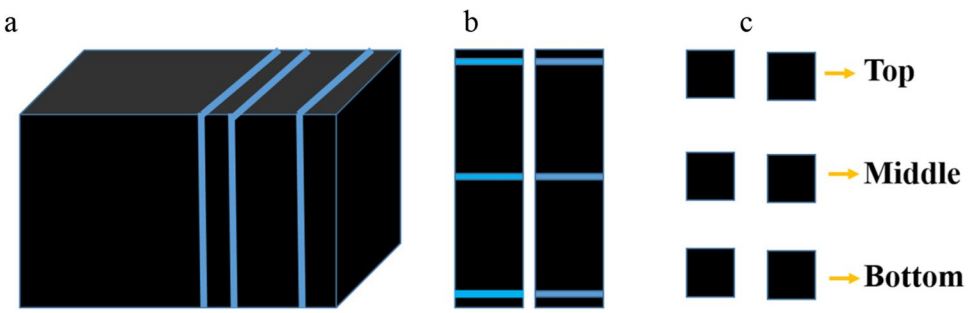


**Fig. 16** Wafer collection to the grown ingot. **a**. grown mc-Si ingot, **b**. corner and centre portion of the brick and **c**. wafer collected from the brick for different zone

## 6 Conclusion

Oxygen concentration and carbon concentration in the grown mc-Si ingot are reduced by increasing the AGFR. After 20 LPM, the SiO gas in the melt-free surface gets reduced from 6.9E2 to 5.1E1ppma. In the melt-free surface, AGFR affects the formation of CO gas and its back diffusion. The CO gas concentration is lower than 3.9E1 ppma. The concentration of oxygen and carbon in grown ingots are 1.5E15 to 9.5E17 atoms/cm$^3$ and 1.5E16 to 2.2E17 atoms/cm$^3$ respectively. The higher value of oxygen and carbon concentration is in very small portion which is present in the red zone of the grown mc-Si ingot. 20 LPM is better for growing the ingot within the critical limit for SiC formation. 25 LPM is better to grow the ingot within the critical limit for the LID formation. Based on the simulation investigation experimentation has been done with the 25 LPM AGFR. From the FTIR spectrum carbon and oxygen concentration of the wafer is calculated. These results are similar to the simulation results. Based on the simulation and experimental analysis 25 LPM AGFR gives better results for the PV application.

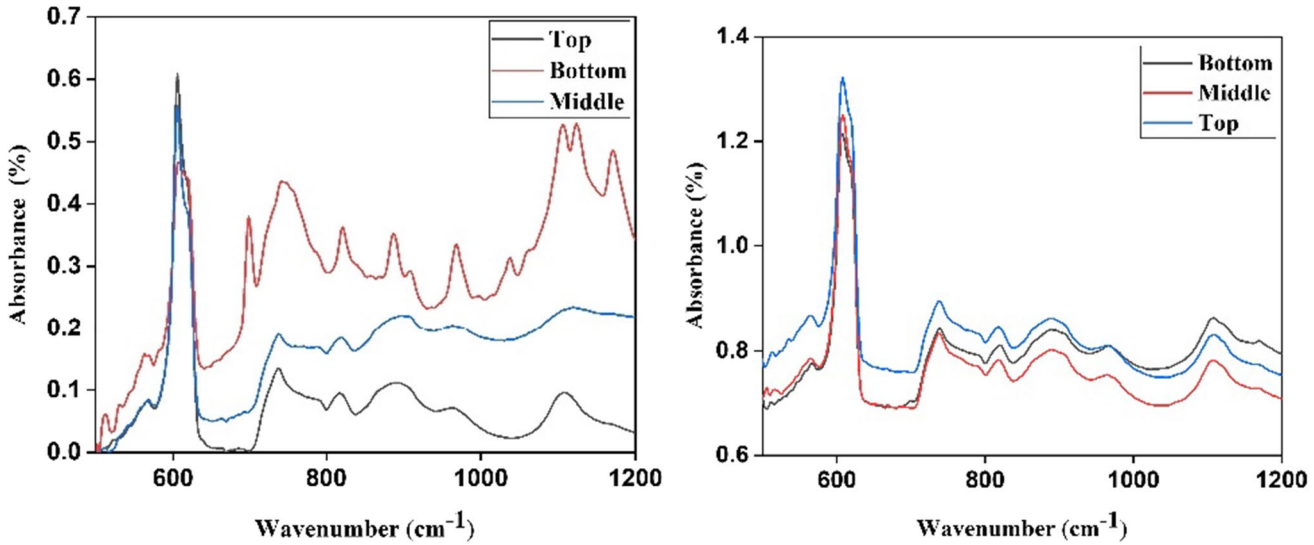


**Fig. 17** FTIR spectra for impurity concentration. The left side is the Corner region of the wafer and the right side is the Centre region of the wafer

**Table 2** Carbon and oxygen impurity concentration of the wafer

| Zone | Position | Carbon concentration (1E16 atoms/cm$^3$) | Oxygen concentration (1E17 atoms/cm$^3$) |
|---|---|---|---|
| Corner | Top | 5.7435 | 0.3479 |
| | Middle | 5.2669 | 0.8481 |
| | Bottom | 4.4067 | 1.9041 |
| Centre | Top | 5.0633 | 0.1650 |
| | Middle | 4.9064 | 0.1789 |
| | Bottom | 4.7526 | 0.5434 |

**Acknowledgements** This work is supported by the Department of Science and Technology, Government of India (Order No. DST/TMD/CERI/RES/2020/7 dated 31/12/2020).

**Authors' Contributions** S. Sugunraj *Conceptualization, Methodology, Formal analysis, Investigation, Data Curation, Resources, Writing - Original Draft, Writing - Review & Editing*
G. Aravindan *Methodology, Formal analysis, Investigation*
M. Srinivasan *Supervision, Visualization*
P. Ramasamy *Supervision*

**Funding** This work is supported by the Department of Science and Technology, Government of India (Order No. DST/TMD/CERI/RES/2020/7 dated 31/12/2020).

**Data Availability** Not applicable.

## Declarations

**Compliance with Ethical Standards** Not Applicable.

**Consent to Participate** Not Applicable.

**Consent for Publication** Not Applicable.

**Conflicts of Interest/Competing Interests** The authors have no conflicts of interest to declare that are relevant to the content of this article.

## References

1. Green M, Dunlop E, Hohl-Ebinger J, Yoshita M, Kopidakis N, Hao X (2021) Solar cell efficiency tables (version 57). Prog Photovolt Res Appl 29(1):3–15
2. Li Z, Liu L, Liu X, Zhang Y, Xiong J (2012). J Crts Growth 360:87–91
3. Wang S, Fang HS, Zhao CJ, Zhang Z, Zhang MJ, Int JFX (2015). J Heat Mass Transf 84:370–375
4. Machida N, Suzuki Y, Abe K, Ono N, Kida M, Shimizu Y (1998). J. Crst. Growth 186(3):362–368
5. Su W, Li J, Li C, Yang W, Wang J (2021). Silicon:1–7
6. Li Z, Liu L, Ma W, Kakimoto K (2011). J. Crst. Growth 318(1):298–303
7. Bellmann MP, Lindholm D (2014). J Crst Growth 399:33–38
8. Li X, Yang Y-C, Hsu C-M, Tseng H-W, Zhang J, Yang C-F (2021). Sensors and Materials 33(8):2607–2618

9. Nakano S, Liu LJ, Chen XJ, Matsuo H, Kakimoto K, Crst J (2009). Growth 311(4):1051–1055
10. Kumar M, Avinash MS, Ramasamy P (2020). Silicon:1–10
11. Ida Z, Chen J-C, Nguyen THT (2018) In MATEC Web of Conferences, vol. 204, p. 05013. EDP Sciences,
12. Gao B, Nakano S, Kakimoto K (2011). J Crst Growth 318(1):255–258
13. Qi X, Liu L, Ma W (2017). J. Crst. Growth 468:933–938
14. Saitoh T, Wang X, Hashigami H, Abe T, Igarashi T, Glunz S, Rein S et al (2001). Sol Energy Mater Sol Cells 65(1–4):277–285
15. Kesavan V, Srinivasan M, Ramasamy P (2019) The influence of multiple-heaters on the reduction of impurities in mc-Si for directional solidification. *silicon* 11(3):1335–1344
16. Gao B, Nakano S, Kakimoto K (2013) Reduction of oxygen impurity in multicrystalline silicon production. Int J Photoener 2013
17. Sanmugavel S, et al. (2017) "Effect of heater design on the melt crystal interface." AIP Conf Proceed. Vol. 1832. No. 1. AIP Publishing LLC,
18. Vorob'ev AN, Sid'ko AP, Kalaev VV (2014). J. Crst. Growth 386:226–234
19. Lan CW, Hsu C, Nakajima K (2015) In handbook of crystal growth. Elsevier, pp 373–411
20. Giannattasio A, Senkader S, Azam S, Falster RJ, Wilshaw PR (2003). Microelectron Eng 70(1):125–130
21. Matsuo, H., Ganesh, R. B., Nakano, S., Liu, L., Kangawa, Y., Arafune, K., ... & Kakimoto, K. J. Crst. Growth, (2008), 310(22), 4666–4671
22. Kerkar F, Kheloufi A, Dokhan N, Ouadjaout D, Belhousse S, Medjahed S, Laib K (2020). Silicon 12(3):473–478
23. Lindroos J, Savin H (2016). Sol Energy Mater Sol 147:115–126
24. Hull R Ed. (1999) Properties of crystalline silicon (no. 20. IET)
25. Xi Z, Tang J, Deng H, Yang D, Que D (2007). Sol Energy Mater Sol 91(18):1688–1691
26. Smirnov AD, Kalaev VV (2008). J Crst Growth 310(12):2970–2976
27. Liu X, Yan G, Hong R (2015). J Mater Sci Technol 31(11):1094–1100
28. Kolbesen BO, Mühlbauer A (1982) Solid state. Electron Lett 25(8):759–775
29. Akiyama N, Yatsurugi Y, Endo Y, Imayoshi Z, Nozaki T (1973). Appl Phys Lett 22(12):630–631
30. Sivaraj D, Kesavan V, Keerthivasan T, Kumar MA, Srinivasan M, Ramasamy P (2022) Investigation of orientation, surface morphology, impurity concentration and reflectivity of the multicrystalline silicon wafers. Mat Chem Phys 125932